Early version, also known as pre-print

A Cenozoic record of the equatorial Pacific carbonate compensation depth

Heiko Pälike [1], Mitchell W. Lyle [2], Hiroshi Nishi [3], Isabella Raffi [4], Andy Ridgwell [5], Kusali Gamage [6], Adam Klaus [6], Gary Acton [7], Louise Anderson [8], Jan Backman [9], Jack Baldauf [2], Catherine Beltran [10], Steven M. Bohaty [1], Paul Bown [11], William Busch [12], Jim E.T. Channell [13], Cecily O. J. Chun [1,22,55], Margaret Delaney [14], Pawan Dewangan [15], Tom Dunkley Jones [16,53], Kirsty M. Edgar [1,54], Helen Evans [17], Peter Fitch [16], Gavin L. Foster [1], Nikolaus Gussone [18], Hitoshi Hasegawa [19], Ed C. Hathorne [20], Hiroki Hayashi [21], Jens O. Herrle [22,55], Ann Holbourn [23], Steve Hovan [24], Kiseong Hyeong [25], Koichi Iijima [26], Takashi Ito [27], Shin-ichi Kamikuri [28,49], Katsunori Kimoto [29], Junichiro Kuroda [30], Lizette Leon-Rodriguez [31], Alberto Malinverno [17], Ted C. Moore Jr. [32], Brandon H. Murphy [33], Daniel P. Murphy [2,1], Hideto Nakamura [28], Kaoru Ogane [34], Christian Ohneiser [35], Carl Richter [36], Rebecca Robinson [37], Eelco J. Rohling [1], Oscar Romero [38], Ken Sawada [28], Howie Scher [39], Leah Schneider [40], Appy Sluijs [41], Hiroyuki Takata [42], Jun Tian [43], Akira Tsujimoto [44], Bridget S. Wade [45,46], Thomas Westerhold [47], Roy Wilkens [48], Trevor Williams [17], Paul A. Wilson [1], Yuhji Yamamoto [49], Shinya Yamamoto [50], Toshitsugu Yamazaki [51] & Richard E. Zeebe [52]

1 Ocean and Earth Science, National Oceanography Centre Southampton, University of Southampton, Waterfront Campus, European Way, Southampton, SO14 3ZH, UK.

2 Department of Oceanography, Texas A&M University, College Station TX 77840-3146, USA.

3 The Center for Academic Resources and Archives, Tohoku University Museum, Tohoku University, Aramaki Aza Aoba 6-3, Aoba-ku, Sendai, 980-8578, Japan.

4 Dipartimento di Geotecnologie per l'Ambiente e il Territorio, DiGAT–CeRS Geo, Universitá "G. DAnnunzio", Campus Universitario, via dei Vestini 31, Chieti Scalo, Italy.

5 School of Geographical Sciences, University of Bristol, University Road, Bristol BS8 1SS, UK.

6 Integrated Ocean Drilling Program, Texas A&M University, 1000 Discovery Drive, College Station TX 77845-9547, USA.

7 Department of Geology, University of California, Davis, One Shields Avenue, Davis CA 95616, USA.

8 Department of Geology, University of Leicester, Leicester LE1 7RH, UK.

9 Department of Geological Sciences, Stockholm University, SE-10691 Stockholm, Sweden.

10 Laboratoire Biominéralisations et Paléoenvironnements (UPMC), Université Pierre et Marie Curie, Case 1164 Place Jussieu, 75252 Paris, France.

11 Earth Sciences, University College London, Gower Street, London WC1E 6BT, UK.

12 Earth and Environmental Sciences, University of New Orleans, 2000 Lakeshore Drive, New Orleans LA 70148, USA.

13 Department of Geological Sciences, University of Florida, 241 Williamson Hall, Gainesville FL 32611-2120, USA.

14 Ocean Sciences, University of California, Santa Cruz, 1156 High Street, Santa Cruz CA 95064, USA.

15 National Institute of Oceanography, Dona Paula, Goa 403 004, India.

16 Imperial College London, Department of Earth Science and Engineering, South Kensington Campus, London, SW7 2AZ, UK.

17 Borehole Research Group, LDEO, Columbia University, PO Box 1000, 61 Route 9W,Palisades NY 10964, USA.

18 Institut für Mineralogie, Westfälische Wilhelms-Universität Münster, Corrensstrasse 24, 48149 Münster, Germany.

19 Department of Natural History Science, Graduate school of Science, Hokkaido University, N10, W8, Kita-ku, Sapporo 060-0810, Japan

20 GEOMAR, Helmholtz Centre for Ocean Research Kiel, Wischhofstrasse 1-3, 24148 Kiel, Germany.

21 Interdisciplinary Faculty of Science and Engineering, Shimane University, 1060 Nishikawatsucho, Matsue City, Shimane 690-8504, Japan.

22 Institute of Geosciences, Goethe University Frankfurt, Altenhöferallee 1, D-60438 Frankfurt, Germany.

23Institut für Geowissenschaften, Christian-Albrechts-Universität zu Kiel, Olhausenstrasse 40, 24098 Kiel, Germany.

24 Department of Geoscience, Indiana University of Pennsylvania, 114 Walsh Hall, Indiana PA 15705, USA.

25 Deep Sea Resources Research Center, Korea Ocean Research and Development Institute, ANSAN PO Box 29, Seoul 425-600, Korea.

26 Institute of Biogeosciences, Japan Agency for Marine-Earth Science and Technology, 2-15 Natsushima-cho, Yokosuka 237-0061, Japan.

27 Faculty of Education, Ibaraki University, 2-1-1 Bunkyo, Mito, Ibaraki 310-8512, Japan.

28 Faculty of Science, Division of Natural History Sciences, Hokkaido University, Kita-10, Nishi-8, Kita-ku, Sapporo 060-0810, Japan.

29 Research Institute for Global Change (RIGC), JAMSTEC, 2-15 Natsushima-Cho, Yokosuka 237-0061, Japan.

30 Institute for Frontier Research on Earth Evolution (IFREE), JAMSTEC, 2-15 Natsushima-cho, Yokosuka 237-0061, Japan.

31 Department of Earth Science, Rice University, 6100 Main Street, MS-126, Houston TX 77005, USA.

32 Department of Geological Sciences, University of Michigan, 1100 North University, Ann Arbor MI 48109-1005, USA.

33 Earth and Planetary Sciences, University of California, Santa Cruz, 1156 High Street, Santa Cruz CA 95064, USA.

34 Institute of Geology and Paleontology, Tohoku University, Aoba 6-4, Aramaki, Aoba-ku, Sendai City 980-8578, Japan.

35 Department of Geology, University of Otago, PO Box 56, Dunedin, New Zealand.

36 Department of Geology and Energy Institute, University of Louisiana, PO Box 44530, Lafayette LA 70504-0002, USA.

37 Graduate School of Oceanography, University of Rhode Island, South Ferry Road, Narragansett RI 02882, USA.

38 Instituto Andaluz de Ciencias de la Tierra, Universidad de Granada, Campus Fuentenueva, 18002 Granada, Spain.

39 Department of Geological Sciences, University of South Carolina, 701 Sumter Street, EWS 617, Columbia SC 29208, USA.

40 Department of Geosciences, Pennsylvania State University, 509 Deike Building, University Park PA 16802, USA.

41 Biomarine Sciences, Institute of Environmental Biology, Utrecht University, Laboratory of Palaeobotany and Palynology, Budapestlaan 4, 3584CD Utrecht, The Netherlands.

42 BK21 Coastal Environmental System School, Division of Earth Environmental System, Pusan National University, San 30 Jangjeon-dong, Geumjeong-gu, Busan 609-735, Korea.

43 Laboratory of Marine Geology, Tongji University, Siping Road 1239, Shanghai 200092, PR China.

44 Faculty of Education, Shimane University, 1060 Nishikawatsucho, Matsue City, Shimane 690-8504, Japan.

45 Department of Geology & Geophysics, Texas A&M University, College Station TX 77843-3115, USA.

46 School of Earth and Environment, University of Leeds, Woodhouse Lane, Leeds, LS2 9JT, UK.

47 Center for marine Environmental Sciences (MARUM), University of Bremen, PO Box 330440, 28334 Bremen, Germany.

48 Hawaii Institute of Geophysics and Planetology, University of Hawaii at Manoa, 1680 East West Road, Honolulu HI 96822, USA.

49 Center for Advanced Marine Core Research, Kochi University, Kochi 783-8502, Japan.

50 Yamanashi Institute of Environmental Sciences, 5597-1 Kenmarubi, Kamiyoshida, Fujiyosida, Yamanashi 403-0005, Japan

51 Geological Survey of Japan, AIST, 1-1-1 Higashi, Tsukuba, Ibaraki 305-8567, Japan.

52 School of Ocean and Earth Science and Technology, Department of Oceanography, University of Hawaii at Manoa, 1000 Pope Road, MSB 504, Honolulu, Hawaii 96822, USA.

53 School of Geography, Earth and Environmental Sciences, University of Birmingham, Edgbaston, Birmingham B15 2TT, UK.

54 School of Earth and Ocean Sciences, Cardiff University, Main Building, Park Place, Cardiff CF10 3AT, UK.

55 Biodiversity and Climate Research Centre (BIK-F) & Senckenberg Gesellschaft für Naturforschung, D-60325 Frankfurt, Germany.

Atmospheric CO_2 concentrations and climate are regulated on geological time scales by the balance between carbon input and its removal by weathering feedbacks involving the erosion of silicate and organic carbon bearing rocks, which also controls the depth in the oceans at which carbonate is dissolved. Here

we present a new carbonate accumulation record that covers the past 53 million years from a depth transect in the equatorial Pacific. The compensation depth tracks long-term ocean cooling, deepening from 3.0–3.5 km during the early Cenozoic to 4.6 km at present, consistent with an overall Cenozoic increase in weathering. We find large superimposed carbonate compensation fluctuations during the middle and late Eocene. Using Earth System models, we identify changes in weathering and the mode of organic carbon delivery as two key processes to explain these large-scale Eocene fluctuations of the carbonate compensation depth.

The Pacific, as the world's largest ocean, is intricately involved in the prominent changes in the global carbon cycle and climate system that took place during the Cenozoic[1]. The equatorial Pacific has a disproportionally large global contribution to biogenic sediment burial in the pelagic realm due to equatorial upwelling, and thus plays an important role in climate regulation[1]. Integrated Ocean Drilling Program (IODP) Expeditions 320/321, the "Pacific Equatorial Age Transect" (PEAT), exploited the northward Pacific plate trajectory during the Cenozoic to recover a continuous sediment sequence from the equatorial Pacific. Eight sites were cored from the sea-floor to basaltic basement, that is aged between 53 and 18 million years before present (Ma), near the past position of the Equator at successive crustal ages on the Pacific plate[2]. Together with previous Deep Sea Drilling Project and Ocean Drilling Program drill cores, these sediments allow reconstruction of changes in the state, nature and variability of the global carbon cycle and climate system in unprecedented detail, from directly after the period of maximum Cenozoic warmth, through the onset of major glaciations, to the present.

Atmospheric CO_2 concentrations and climate are regulated on geological time scales by volcanic and metamorphic outgassing, weathering feedbacks involving the weathering of silicate and organic carbon bearing rocks, and carbonate and organic

carbon burial[3,4]. The integrated effect of these processes dictates the carbonate saturation state of the oceans that is reflected in the carbonate compensation depth (CCD), which has been highly influential in understanding past changes in the marine carbon cycle[5,6]. The CCD is a sediment property and occurs in the oceans where the downward flux of carbonate rain delivered from calcifying organisms is balanced by dissolution (Fig. 1), so that little or no carbonate is preserved in sediments below this depth. The CCD can be reconstructed using sediment cores[5-8].

Here we determine the evolution of the CCD in unprecedented resolution by establishing the variation of net carbonate accumulation rates with respect to palaeo-depth at multiple sites, using a common chronology and stratigraphic correlation. We then use carbon cycle models to explore viable mechanisms that may be responsible for the observed CCD variations, highlighting the importance of weathering supply of solutes to the deep ocean, and changes in the partitioning of organic matter delivery to deep-sea sediments into a labile and refractory component.

A Cenozoic CCD record

Our new reconstruction of how the Cenozoic CCD in the equatorial Pacific region evolved through the Cenozoic is shown in Fig. 2 (suppl. Fig. S1 shows this as a plot of mass accumulation rate against age and palaeo-latitude, suppl. Fig. S2 shows an enlarged version for the Eocene). The evolving palaeo-position of the CCD is determined where the carbonate accumulation rates interpolated across the palaeo-depth transect reach zero as a function of depth. Overall, the CCD tracks ocean cooling[9], with a deepening from 3–3.5 km during the early Cenozoic to 4.6 km at present, consistent with findings of an overall Cenozoic increase in silicate weathering[10-13]. Superimposed on this overall deepening are repeated large CCD fluctuations during the middle and late Eocene.

We find that during the earliest Eocene (~56–53 Ma), the equatorial CCD generally occurred at a palaeo-depth of around 3.3–3.6 km, with superimposed "hyperthermal"-related CCD shoaling events[9,14]. Between ~52 and 47 Ma the CCD reached depths as shallow as 3 km, coincident with the Early Eocene Climatic Optimum (EECO)[15] when atmospheric CO_2 concentrations, including their uncertainty bounds, reached an estimated ~1,100–3,000 ppmV[16], and the lowest benthic oxygen isotope values (indicating peak deep-ocean temperature) throughout the Cenozoic were attained[15].

From ~46–34 Ma our record reveals a fluctuating and highly variable CCD[8], resolving 5–7 CCD deepenings and carbonate accumulation events (CAE) with durations of several hundred thousand years to 1 Myr, interrupted by rapid CCD shoalings with an amplitude of ~0.5-1.0 km (CAE-1 to CAE-7; Fig. 2). The largest magnitude fluctuation of the CCD during the middle and late Eocene coincided with carbonate accumulation event 3 (CAE-3)[8], followed by a near 1 km shoaling that is coeval with the Middle Eocene Climatic Optimum (MECO)[17,18]. A sustained large deepening (>1 km) then terminated a late Eocene interval of variability and coincided with the Eocene/Oligocene (E/O) transition[19]. This terminal early Oligocene CCD deepening was contemporaneous with ice sheet growth, sea-level fall, and a shift in carbonate deposition from shallow to deep waters[19,20]. The deeper (~4.6 km) and apparently more stable CCD of the Oligocene was interrupted again in the Miocene at ~18.5 Ma by a ~600 m shoaling, lasting around 2.5 million years, which was previously described as the "carbonate famine"[6]. The CCD deepened again to around 4.7 km at ~16 Ma as a consequence of increased carbonate productivity[6]. For the deepening event at ~16 Ma the analysis of the PEAT data alone are complicated by the latitudinal movement of some sites (U1332–U1334) outside of the Pacific equatorial zone (suppl. Fig. S1). However, the interpretation is supported by previous work[6] and corroborated by large increases in carbonate mass accumulation rates at shallower depths of Sites U1335, U1337 and U1338 (Fig. 2). An interval with the

deepest equatorial Pacific Cenozoic CCD of around 4.8 km was terminated by shoaling at ~10.5 Ma in a rapid "carbonate crash" event[21]. For the remainder of the Neogene, the equatorial Pacific CCD resided around 4.5 km depth with superimposed fluctuations in carbonate accumulation related to shorter-term climatic oscillations on Milankovitch time scales (20-400 kyr), as well as to the periodic deposition of diatom mats[2].

Eocene CCD fluctuations

Two features of the equatorial Pacific CCD behaviour during the Cenozoic stand out and demand further investigation. First, the Eocene CCD resided at an average depth of around 3.5 km, or ~1 km shallower than during post-Eocene time, with a geologically rapid and permanent deepening at the E/O transition. The E/O CCD deepening has previously been ascribed to ice expansion on Antarctica and sea-level fall, driving a shelf-to-basin shift in carbonate partitioning[19,20]. In contrast, for Eocene CAEs we lack evidence[22] for large bi-polar fluctuations in ice volume, so that alternative mechanisms must be explored.

Second, the middle to late Eocene was characterised by five major CCD fluctuations that lasted between 250 kyr and 1 Myr and had amplitudes between 200 and 900 meters. The ~900 m CCD shoaling at ~40.5 Ma, a globally recognised feature[17] associated with the transition from CAE-3 to MECO, approaches the amplitude but is opposite in sign to the CCD shift during the E/O transition from greenhouse to icehouse. We currently lack a definite confirmation that other CAEs are represented in records outside of the equatorial Pacific, primarily due to the scarcity of continuous, well-dated pelagic sedimentary records at an array of palaeo-depth positions, but we note that data from ODP Site 929E in the equatorial Atlantic tentatively support our hypothesis of CAEs as global features (suppl. Fig. S3). In the equatorial Pacific, carbonate accumulation events (CAEs) coincided with increased biogenic silica accumulation rates and shifts between calcareous and siliceous

microfossils[8,18]. CAEs also coincided with enhanced burial of organic carbon in an

Eocene Pacific Ocean otherwise characterised by productivity similar to today but

with much faster water-column recycling; these increases in organic carbon burial

start from a much lower Eocene baseline of C_{org} preserved in sediments, averaging

only one tenth of the present day value[8,23-25].

Carbon system modelling

To quantitatively explore the potential of different processes to generate the CCD

signal reconstructed for the middle to late Eocene, we made use of steady-state results

from an Earth System Model of Intermediate Complexity (*GENIE*)[26,27], and

investigated non-steady-state behaviour of shorter-lived processes with the palaeo-

configuration of the *LOSCAR* box model[28] (suppl. material). Overall, the results from

both models significantly reduce the number of possible mechanisms that are

consistent with the reconstructed CCD history, either by demonstrating that a number

of possible processes are not able to sustain large CCD changes over long enough

time periods (>250 kyr), or by inconsistency with other proxy observations.

We start by assuming that middle–late Eocene CCD fluctuations represent

alternating steady states of marine carbon cycling and that all carbonate weathering

and climate feedbacks had time to operate and equilibrate. The justification for this is

that the typical silicate weathering compensation time is of the order of ~0.1 Myr [4,29],

much shorter than the duration of the reconstructed CCD fluctuations (0.25–1 Myr;

Fig. 2). We then test the sensitivity of a range of established hypotheses for changing

the CCD.

Processes we have investigated that either do not appear to be consistent with

reconstructed amplitudes and durations of CCD shifts or are inconsistent with other

proxy evidence (suppl. material) include: (1) C_{org} surface export rain ratio changes,

which we exclude because the resultant CCD variations are too small in comparison to what we observe; (2) a shift in carbonate deposition between the shelf and deep ocean, for which a repeated large-scale oscillation in ice mass would be required that has so far not been observed; (3) a shift of deep ocean ventilation between a dominant Southern Ocean and dominant North Pacific source, which would lead to opposite CCD behaviour in different ocean basins; and (4) changes in deep-sea temperatures and the Mg and Ca concentration of seawater[4,9,30-32] , which both modify the stability of calcium carbonate. For these, the CCD can be affected only by relatively subtle changes in the offset between CCD and lysocline because of the need to ultimately re-balance sources and sinks. We note that we cannot completely rule out the potential for ventilation changes to be compatible with our CCD data, and this will need to be resolved by future drilling in the North Atlantic.

Next, we focus on two model scenarios that do have the potential to sustain CCD changes of the required duration and amplitude: (1) perturbations to continental weathering and variations in solute input to the deep ocean, driving synchronous changes in CCD and lysocline depth globally, and/or (2) changes in the partitioning of organic carbon flux between labile and refractory components, affecting both deep-sea carbonate dissolution and the thickness of the lysocline transition zone (and hence partially decoupling the CCD from the lysocline).

To explore the first mechanism, we computed the steady-state CCD position in the equatorial Pacific through a range of atmospheric CO_2 values relative to pre-industrial modern ($1 \times CO_2 = 278$ ppmV) and against a range of solute weathering fluxes of Ca and HCO_3^- to the deep ocean in *GENIE*. Since in *GENIE* the solute flux to the deep ocean is the total weathering flux minus what is deposited on the shelves, changes in solute flux implicitly model either a change of the total flux, or shelf-basin partitioning. Our results (Fig. 3a) indicate that, for a given value of atmospheric CO_2, changes in solute flux to the deep ocean are in principle able to achieve changes in the

equatorial Pacific CCD of the amplitude suggested by observations (several hundred m to >1 km). For the Cenozoic, this supports the initial correlation between increased silicate weathering rates and CCD deepening.

However, other carbon cycle impacts resulting from the assumed driver of changes in solute supply must also be considered. On <1 Myr time scales, tectonic uplift is too slow, and there is no convincing evidence for repeated large-scale sea level fluctuations during the middle-to-late Eocene that could alternately shift the locus of carbonate deposition between shelf and deep ocean. Therefore, increasing solute supply should be coupled to increased weathering, a warmer climate, and higher CO_2, unless changes in orbital configuration significantly enhance or reduce monsoon circulation (at constant CO_2), which could affect weathering fluxes via effects on precipitation intensity and distribution (which is not tested here). Our modelling reveals that increasing atmospheric CO_2 with fixed weathering (i.e. with no weathering–temperature feedback enabled), results in a shallower CCD. This is a consequence of non-linearities in the carbonate system and reflects a deepening of the lysocline at the expense of the CCD and contraction of the lysocline transition zone. When this is combined with the response of increased weathering by activating the full silicate weathering feedback, we find an unexpected result: when progressively increasing the rate of prescribed CO_2 outgassing in a series of *GENIE* experiments, atmospheric CO_2 and weathering flux happen to co-vary in such a way that they result in a largely invariant CCD depth (Fig. 3a). This result is subject to a number of model uncertainties and assumptions, including the degree of non-linearity of weathering with climate, for which we have assumed a simple global-average response[29], and a 1:1 partitioning between carbonate and silicate weathering. This negative feedback in regulating pCO$_2$ on geologic timescales due to weathering of continental materials had been included in the original BLAG[33] modeling study and is also used in *GENIE* and *LOSCAR*, but there are significant uncertainties attached to this parameterisation. For example, the strength of this feedback has been shown to lead to significant

variations in the carbon cycle response to weathering, but remains poorly constrained[29]. While different weathering formulations were not tested with *GENIE*, we predict that the weak relationship between CCD and pCO_2 (Fig. 3a) likely indicates that additional silicate weathering changes in response to temperature will result in only small deviations from an invariant CCD after reaching steady-state. Our results illustrate the non-intuitive nature of CCD behaviour and that higher marine carbonate deposition under a warmer, higher CO_2 climate need not require a deeper observed CCD.

Independent observations of sediment composition and changes of dominant microfossil groups lead us to assess also whether changes in the behaviour of organic matter driving dissolution during the middle–late Eocene played a role. The pertinent observations are shifts between siliceous and calcareous microfossils and an increase of organic carbon burial flux during CAE-3, with simultaneous increased burial fluxes of calcareous and biosiliceous sediment[1,2,23-25]. For example, sediment smear slides from the equatorial Pacific reveal a major increase in diatom content from 0% to near 50% near the end of this event[24]. The relative changes in biogenic opal are much larger than those in calcareous plankton, and indicate major temporal re-organisation of biotic composition rather than simple changes in productivity levels. In addition, the amount of organic carbon preserved in Eocene equatorial Pacific sediments is an order of magnitude smaller than today, despite a productivity that was not very different to the present[8,24], suggesting a more nutrient enriched deep ocean.

We investigate the viability of a "labile organic matter" hypothesis to help explain the CCD fluctuations. We repeat the *GENIE* net-weathering supply analysis but now change the partitioning between 'labile' organic carbon, which is re-dissolved in the upper water-column and drives carbonate dissolution, and refractory organic carbon, which reaches the sea-floor and is available for further re-mineralisation or carbon burial. This modifies the ocean's dissolved inorganic carbon

as well as the net carbonate preservation flux[34]. This hypothesis builds on, but differs from the classic glacial CO_2 "rain rate" hypothesis[35], which postulated that changes in the $CaCO_3$ flux to ocean sediments, at a fixed particulate organic carbon (POC) supply, could be an effective way of changing atmospheric CO_2. However, the rebalancing of sedimentation *versus* weathering – "carbonate compensation" – while helping to drive a potential 60 ppm CO_2 fall for a 40% decrease in $CaCO_3$:POC export ratio, also leads to a CCD that changed relatively little (suppl. Fig. S5). This mechanism may also not be compatible with the consequence of any POC "ballasting" by $CaCO_3$[36,37].

Results for modelling the labile organic matter hypothesis (Fig. 3b) indicate that a smaller initial fraction of labile organic matter results in a net increase in carbonate accumulation in regions of high productivity such as the eastern equatorial Pacific, Southern Ocean, and equatorial Atlantic, due to reduced water column dissolution. Carbonate compensation acts to mitigate the CCD changes but with a spatially heterogeneous pattern, leaving a deeper CCD in the eastern equatorial Pacific (suppl. Fig. S9) and Atlantic, but resulting in smaller changes in the western Pacific. The modelled changes in carbonate accumulation in the eastern equatorial Pacific in this scenario indicate that CCD changes of ~300–600 m are possible for a 2–4 fold change in the initial fraction of labile organic matter (Fig. 3b), roughly equivalent to the amplitude of all but the largest MECO associated fluctuations in the record[17]. Although GENIE does not explicitly distinguish labile from refractory carbon, we are effectively assuming that surface biological productivity and the total flux of POC to deep-sea sediments need not change, but that it is either predominantly available for oxidation and driving carbonate dissolution (labile), or it is largely preserved and buried (refractory) and does not drive substantial additional carbonate dissolution.

CCD buffering

Overall, our modelling also reveals that the CCD is remarkably well buffered against short and long term perturbations of the global carbon cycle. Only a few of the mechanisms commonly envisaged as important in controlling the CCD in practice have the capacity to change the amplitude of the *steady-state* CCD sufficiently and for long enough to be compatible with our reconstruction. In contrast, our labile organic matter hypothesis is consistent with shifts between siliceous and calcareous microfossil groups, and changes in organic carbon preservation and burial[24], and has sufficient amplitude to explain variability during the middle–late Eocene, perhaps in concert with simultaneous weathering flux changes. We note that the initial depth of the CCD may amplify these changes as its response to forcing is a function of the total amount of calcite available to be dissolved over a given depth range of seafloor (suppl. Material and Fig. S4). This suggests a smaller compensation capacity during Eocene time (due to a shallower CCD), which results in a higher sensitivity of carbonate preservation for a given carbon perturbation.

The Pacific CCD record presented here offers a remarkable new view of Cenozoic ocean carbonate chemistry evolution and provides the basis for future quantitative tests of multiple possible controlling mechanisms. The close correspondence of deep-ocean temperatures derived from benthic foraminiferal $\delta^{18}O$ records and the equatorial Pacific CCD is intriguing and suggests a close coupling of climate and carbon cycle feedbacks during the Cenozoic, tied to an overall increase in weathering during the Cenozoic.

Methods summary

Carbonate measurements were performed by coulometry[2], and supplemented with data from ODP and DSDP Legs (Supplementary Table S1). Accumulation rates were determined by using high-resolution age models and bulk dry density measurements.

Stratigraphic correlation of sites was achieved through bio- and magnetostratigraphy, XRF data and physical property measurements[38], adjusted to the agemodel of the PEAT expeditions[2] revised to new site correlations[38]. Present-day site positions were backtracked using published stage poles[2]. Palaeo-depths were computed including backstripping and using standard methodology[6]. The CCD was semi-quantitatively determined by plotting available carbonate accumulation rate data in 250 kyr windows, and fitting a regression line through carbonate accumulation rates decreasing with depth. *GENIE* Earth System modelling was based on Eocene boundary conditions from previous studies[26,27] using a Paleocene palaeobathymetry (model *SVN* revision 6491). Scenarios were investigated as open system runs and with enabled climate feedback (temperature responsive to greenhouse gas forcing) until steady state conditions were achieved (~150 kyr). Ensembles were run on the Southampton high performance computing system *IRIDIS3*. All scenarios were run for atmospheric CO_2 concentrations ranging from 1x to 6x pre-anthropogenic (1×=278 ppmV). The scenario in Fig. 3a ("weathering") varied total weathering fluxes from 25% to 200% of modern DIC values in 25% steps (100%=10 Tmol yr^{-1}) [39]. For all runs bioturbation was switched off to speed up the achievement of steady state. All models were run adding a background wetland CH_4 flux at x5 pre-industrial levels, and with a constant detrital flux of 0.18 g cm^{-2} kyr^{-1}. The net-weathering Scenario in Fig. 3a was then re-run with varying values for the initial fraction of labile organic carbon 'POM2' (standard GENIE value ~5.6%, additional runs with zero, half, double and quadruple standard value), detailed in a previous publication[34]. Additional *GENIE* scenarios are described in the suppl. Material.

Methods

Carbonate measurements were performed by coulometry during IODP Expeditions 320/321[2], and supplemented with previously published data from ODP and DSDP Legs (Supplementary Table S1). Mass and carbonate accumulation rates were determined by using high-resolution age models and bulk dry density measurements.

Stratigraphic correlation of sites was achieved through bio- and magnetostratigraphy, XRF data and physical property measurements[38], and all data are adjusted to the agemodel of the PEAT expeditions[2]. Present-day site positions were backtracked using published stage poles[2]. Palaeo-depths were computed assuming subsidence proportional to the square root of age, following previous approaches[6], starting from an assumed ridge crest depth of 2.75 km, and taking into account sediment loading. Uncertainties in the palaeo-depth history are a function of (1) age control, (2) knowledge of the palaeo-depth of the ridge crest, (3) the subsidence history of drill sites, and (4) the sediment loading history for each site. The vertical uncertainty of palaeo-depth trajectories is likely to be largest for the earliest part of our records, attributable to the initially more rapid thermal cooling and subsidence at the palaeo-ridge (basement age error ±0.5 Myr), and due to absolute uncertainties in the palaeo-depth of the ridge crest (depth error ~±350 m)[40]. Reconstructions become more robust for each site moving forward in time, as the thermal subsidence rate attenuates. We therefore estimate the uncertainty of absolute site palaeo-depths to be of the order of several hundred meters in the early part of the reconstruction for each site, and ~250 m for the remaining record. The palaeo-depth-transect approach however, means that most of the included sites originate from the same Pacific plate ridge segment, thereby reducing the relative error of depth reconstructions. For this study, we assumed a palaeo-depth of the ridge of 2.75 km, fitted subsidence parameters according to the determined basement age and present-day depth and backstripped the sediment loading following previous work[6]. Age models for individual sites are based on an integrated palaeomagnetic and biostratigraphic framework largely following the Expedition dates[2], but revised to new site correlations[38]. Biostratigraphic ages from previous ODP and DSDP sites were updated to this age framework. The new carbonate compensation depths were semi-quantitatively determined by plotting available carbonate accumulation rate data in 250 kyr windows, and fitting a regression line through the carbonate accumulation rates that are decreasing with depth. *GENIE* Earth System modelling was based on previous studies[26,27] using a

Paleocene palaeobathymetry, using model SVN revision 6491. Scenarios were investigated as open system runs and with enabled climate feedback (temperature responsive to greenhouse gas forcing) until steady state conditions were achieved (~150 kyr), using Eocene boundary conditions[27] (a solar constant reduced by 0.46% for Palaeogene time (1,361.7 Wm^{-2}; a reduced salinity of 33.9 psu; a constant $CaCO_3$:C_{org} ratio of 0.2, and with seawater concentrations of Mg≈30 mmol kg^{-1} and Ca≈15 mmol kg^{-1}. Ensembles were run on the Southampton high performance computing system *IRIDIS3*. All scenarios were run for atmospheric CO_2 concentrations ranging from 1x to 6x pre-anthropogenic (1×=278 ppmV). Bottom water temperatures in the model runs corresponding to increasing CO_2 levels are 6.6, 9.4, 11.1, 12.3, 13.3, and 14.2ºC, respectively. For all runs bioturbation was switched off to speed up the achievement of steady state. All models were run adding a background wetland CH_4 flux at x5 pre-industrial levels, and with a constant detrital flux of 0.18 g cm^{-2} kyr^{-1}. The scenario in Fig. 3a ("weathering") varied total weathering fluxes from 25% to 200% of modern DIC values in 25% steps (100%=10 Tmol yr^{-1})[39]. The net-weathering Scenario in Fig. 3a was then also re-run with varying values for the initial fraction of labile organic carbon parameter 'POM2' (detailed in[34], standard GENIE value ~5.6%, additional runs with zero, half, double and quadruple standard value). Results from further *GENIE* scenario runs not resulting in large CCD changes (rain ratio and Mg/Ca changes) are detailed in the suppl. Material), and we also include a description of transient model runs using the *LOSCAR* box model[28]. For the supplementary "rain ratio" scenario we varied $CaCO_3$:C_{org} ratios from 0.1 to 0.225 in 0.025 steps, using a fixed 50% modern weathering supply to the deep ocean. A supplementary "Mg/Ca" scenario varied seawater Mg and Ca concentrations using previously published values[32] for a Mg/Ca range from 1.3 to 5.1, also using a 50% weathering flux compared to modern.

'**Supplementary Information** accompanies the paper on **www.nature.com/nature**.'

Author Contributions HP and AR wrote the manuscript. All authors contributed to interpretation and

manuscript edits and discussions.

Author Information Reprints and permissions information is available at **www.nature.com/reprints**.

The authors declare no competing financial interests. Correspondence and requests for materials should

be addressed to heiko@noc.soton.ac.uk.

Figure 1 Conceptual figure illustrating the position of the CCD and lysocline, and their relationship to ocean bathymetry, carbonate accumulation rate and $CaCO_3$ content. The CCD, a sediment property, is defined where carbonate rain is balanced by carbonate dissolution. Previously, it has been operationally defined to coincide with a fixed %$CaCO_3$ content (e.g., 10%) in sediments[5], or where carbonate accumulation rate interpolates to zero[6] (This second definition is advantageous as it is independent of noncarbonate supply or dilution effects). The lysocline is the horizon where dissolution becomes first noticeable (a sediment property), and is typically below the calcite saturation horizon.

Figure 2 Equatorial Pacific total and carbonate accumulation rate history as a function of age and palaeo-depth. Circle area is scaled by accumulation rate. Filled circles are for carbonate accumulation rates, outlined circles mark total mass accumulation rate including non-carbonate components. Carbonate accumulation rates are plotted as a function of

geological age at the backtracked and unloaded palaeo-water depth. Data are plotted with a lighter colour where the palaeo-latitude falls outside of a ±3.5° band around the palaeo-equator. The palaeomagnetic polarity age scheme used[2] is shown above age-scale. The position of the equatorial Pacific CCD is indicated by a solid red line. Dashed line in the early Eocene marks reconstruction from off-equatorial sites. Data displayed against age and palaeo-latitude are given in suppl. Fig. S1. Middle panels display 5 point moving average benthic oxygen and carbon isotope values from a global compilation[9]. Bottom panel shows an atmospheric CO_2 compilation modified from[16,41], plotted on a logarithmic CO_2 scale relative against pre-industrial CO_2 (1x=278 ppmV).

Figure 3 *GENIE* **steady state model CCD results. a**, shown contoured as a function of atmospheric CO_2 concentrations and total net deep-sea weathering flux (compared to modern). All models were run without direct feedback on silicate weathering. The red lines indicate what the increase in weathering flux would be when moving from 1x to 6x CO_2 when silicate weathering feedback is enabled (using a partitioning of total initial weathering into silicate and carbonate weathering in a 1:1 ratio). For example, starting at 100% weathering flux at 1xCO_2 and increasing CO_2 results in additional silicate and carbonate weathering which increases the total modelled deep-ocean solute flux, and has the potential to compensate CCD changes that result from the enhanced CO_2 alone. **b**, as a, but plotting CCD as function of CO_2 and initial fraction of labile C_{org}. This model ensemble was run with 100% net weathering compared to modern, and a surface $CaCO_3$:C_{org} rain ratio of 0.2. A global change of C_{org} results in opposite effects on carbonate preservation in the high-productivity eastern Pacific and Atlantic compared to low-productivity regions.

1   Lyle, M. *et al.* Pacific ocean and Cenozoic evolution of climate. *Reviews of Geophysics* **46**, RG2002, doi:10.1029/2005RG000190 (2008).

2   Pälike, H., Nishi H. Lyle M. Raffi I. Gamage K. Klaus A. and the Expedition 320/321 Scientists. *Proc. IODP 320/321. Integrated Ocean Drilling Program Management International, Inc.*, (2010).

3   Broecker, W. S. & Peng, T.-H. The role of CaCO3 compensation in the glacial to interglacial atmospheric CO2 change. *Global Biogeochemical Cycles* **1**, 15-29, doi:10.1029/GB001i001p00015 (1987).

4   Ridgwell, A. & Zeebe, R. The role of the global carbonate cycle in the regulation and evolution of the Earth system. *Earth and Planetary Science Letters* **234**, 299-315, doi:10.1016/j.epsl.2005.03.006 (2005).

5   Van Andel, T. H., Heath, G. R. & Moore Jr., T. C. Cenozoic history and paleoceanography of the central equatorial Pacific Ocean : a regional synthesis of Deep Sea Drilling Project data. *Geol. Soc. Am. Memoir* **143**, 1-134 (1975).

6   Lyle, M. Neogene carbonate burial in the Pacific Ocean. *Paleoceanography* **18**, 1059, doi:10.1029/2002PA000777 (2003).

7   Peterson, L. C. & Backman, J. in *Proc. Ocean Drill. Prog., Sci. Results* Vol. 115 (eds R. A. Duncan, J. Backman, L. C. Peterson, & others) 467-508 (Ocean Drilling Program, 1990).

8   Lyle, M. W., Olivarez Lyle, A., Backman, J. & Tripati, A. in *Proc. Ocean Drill. Prog., Sci. Results* Vol. 199 (eds P.A. Wilson, M. W. Lyle, & J.V. Firth) 1-35 (Ocean Drilling Program, TX, 2005).

9   Zachos, J. C., Dickens, G. R. & Zeebe, R. E. An early Cenozoic perspective on greenhouse warming and carbon-cycle dynamics. *Nature* **451**, 279-283, doi:10.1038/nature06588 (2008).
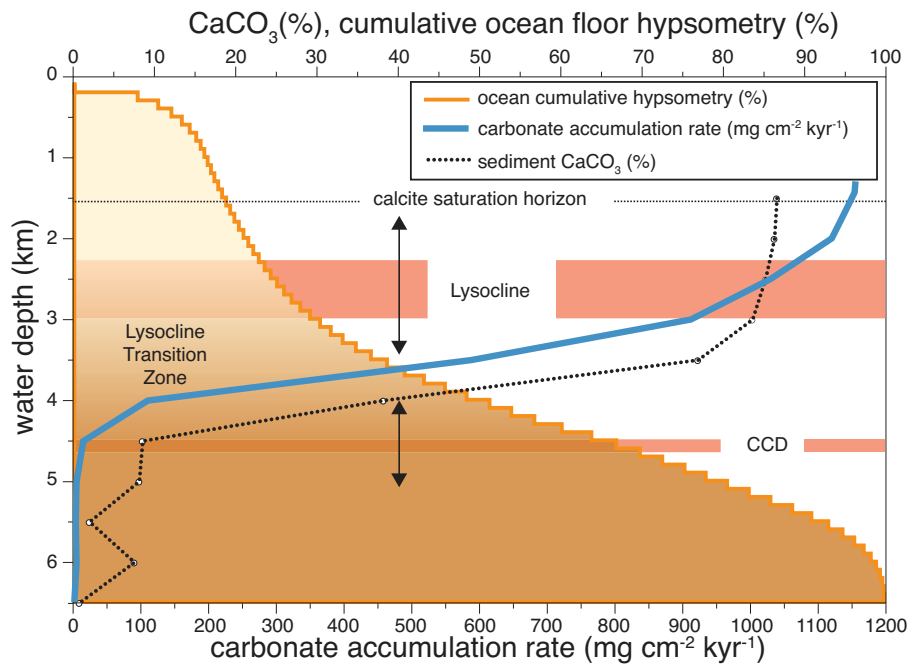
10   Edmond, J. M. Himalayan Tectonics, Weathering Processes, and the Strontium Isotope Record in Marine Limestones. *Science* **258**, 1594-1597 (1992).

11   Lear, C. H., Elderfield, H. & Wilson, P. A. A Cenozoic seawater Sr/Ca record from benthic foraminiferal calcite and its application in determining global weathering fluxes. *Earth and Planetary Science Letters* **208**, 69-84, doi:Doi 10.1016/S0012-821x(02)01156-1 (2003).

12   Misra, S. & Froelich, P. N. Lithium Isotope History of Cenozoic Seawater: Changes in Silicate Weathering and Reverse Weathering. *Science*, doi:10.1126/science.1214697 (2012).

13   Peucker-Ehrenbrink, B. & Ravizza, G. The marine osmium isotope record. *Terra Nova* **12**, 205-219 (2000).

14   Leon-Rodriguez, L. & Dickens, G. R. Constraints on ocean acidification associated with rapid and massive carbon injections: The early Paleogene record at Ocean Drilling Program Site 1215, equatorial Pacific Ocean. *Palaeogeography, Palaeoclimatology, Palaeoecology* **298**, 409-420, doi:10.1016/j.palaeo.2010.10.029 (2010).

15   Zachos, J. C., Pagani, M., Sloan, L., Thomas, E. & Billups, K. Trends, rhythms, and aberrations in global climate 65 Ma to present. *Science* **292**, 686-693, doi:10.1126/science.1059412 (2001).

16   Beerling, D. J. & Royer, D. L. Convergent Cenozoic CO2 history. *Nature Geoscience* **4**, 418-420, doi:10.1038/ngeo1186 (2011).

17   Bohaty, S. M., Zachos, J. C., Florindo, F. & Delaney, M. L. Coupled greenhouse warming and deep-sea acidification in the middle Eocene. *Paleoceanography* **24**, PA2207, doi:10.1029/2008PA001676 (2009).

18   Spofforth, D. J. A. *et al.* Organic carbon burial following the middle Eocene climatic optimum in the central western Tethys. *Paleoceanography* **25**, PA3210, doi:10.1029/2009PA001738 (2010).

19   Coxall, H. K., Wilson, P. A., Pälike, H., Lear, C. H. & Backman, J. Rapid stepwise onset of Antarctic glaciation and deeper calcite compensation in the Pacific Ocean. *Nature* **433**, 53-57, doi:10.1038/nature03135 (2005).

20   Merico, A., Tyrrell, T. & Wilson, P. A. Eocene/Oligocene ocean de-acidification linked to Antarctic glaciation by sea-level fall. *Nature* **452**, 979-983, doi:10.1038/nature06853 (2008).

21   Lyle, M. W., Dadey, K. & Farrell, J. in *Proc. Ocean Drill. Prog., Sci. Results* Vol. 138 (eds N.G. Pisias *et al.*) 821-837 (Ocean Drilling Program, 1995).

22   Edgar, K. M., Wilson, P. A., Sexton, P. F. & Suganuma, Y. No extreme bipolar glaciation during the main Eocene calcite compensation shift. *Nature* **448**, 908-911, doi:10.1038/nature06053 (2007).

23   Moore Jr., T. C., Jarrard, R. D., Olivarez Lyle, A. & Lyle, M. W. Eocene biogenic silica accumulation rates at the Pacific equatorial divergence zone. *Paleoceanography* **23**, doi:10.1029/2007PA001514 (2008).

24   Olivarez Lyle, A. & Lyle, M. W. in *Proc. Ocean Drill. Prog., Sci. Results* Vol. 199 (eds P.A. Wilson, M. W. Lyle, & J.V. Firth) 1-35 (Ocean Drilling Program, TX, 2005).

25   Olivarez Lyle, A. & Lyle, M. W. Missing organic carbon in Eocene marine sediments: Is metabolism the biological feedback that maintains end-member climates? *Paleoceanography* **21**, doi:10.1029/2005PA001230 (2006).

26   Panchuk, K., Ridgwell, A. & Kump, L. R. Sedimentary response to Paleocene-Eocene Thermal Maximum carbon release: A model-data comparison. *Geology* **36**, 315-318, doi:10.1130/G24474A.1 (2008).

27   Ridgwell, A. & Schmidt, D. N. Past constraints on the vulnerability of marine calcifiers to massive carbon dioxide release. *Nature Geoscience* **3**, 196-200, doi:10.1038/NGEO755 (2010).

28   Zeebe, R. E. LOSCAR: Long-term Ocean-atmosphere-Sediment
      CArbon cycle Reservoir Model v2.0.4. *Geoscientific Model
      Development* **5**, 149-166, doi:10.5194/gmd-5-149-2012 (2012).

29   Uchikawa, J. & Zeebe, R. E. Influence of terrestrial weathering on
      ocean acidification and the next glacial inception. *Geophysical
      Research Letters* **35**, L23608, doi:DOI 10.1029/2008GL035963 (2008).

30   Coggon, R. M., Teagle, D. A. H., Smith-Duque, C. E., Alt, J. C. &
      Cooper, M. J. Reconstructing Past Seawater Mg/Ca and Sr/Ca from
      Mid-Ocean Ridge Flank Calcium Carbonate Veins. *Science* **327**, 1114-
      1117, doi:10.1126/science.1182252 (2010).

31   Stuecker, M. F. & Zeebe, R. E. Ocean chemistry and atmospheric CO2
      sensitivity to carbon perturbations throughout the Cenozoic.
      Geophysical Research Letters **37**, L03609,
      doi:10.1029/2009GL041436 (2010).

32   Tyrrell, T. & Zeebe, R. History of carbonate ion concentration over the
      last 100 million years. *Geochimica Et Cosmochimica Acta* **68**, 3521-
      3530, doi:10.1016/j.gca.2004.02.018 (2004).

33   Berner, R. A., Lasaga, A. C. & Garrels, R. M. The carbonate-silicate
      geochemical cycle and its effect on atmospheric carbon dioxide over
      the past 100 million years. *American Journal of Science* **283**, 641-683
      (1983).

34   Ridgwell, A. *et al.* Marine geochemical data assimilation in an efficient
      Earth System Model of global biogeochemical cycling. *Biogeosciences*
      4, 87-104, doi:10.5194/bg-4-87-2007 (2007).

35   Archer, D. & Maier-Reimer, E. Effect of deep-sea sedimentary calcite
      preservation on atmospheric CO2 concentration. *Nature* **367**, 260-263,
      doi:10.1038/367260a0 (1994).

36   Armstrong, R. A., Lee, C., Hedges, J. I., Honjo, S. & Wakeham, S. G. A
      new, mechanistic model for organic carbon fluxes in the ocean: based

on the quantitative association of POC with ballast minerals. *Deep Sea Research Part II: Topical Studies in Oceanography* **49**, 219-236, doi:10.1016/S0967-0645(01)00101-1 (2002).

37   Ridgwell, A. An end to the "rain ratio" reign? *Geochemistry Geophysics Geosystems* **4**, 1051, doi:10.1029/2003GC000512 (2003).

38   Westerhold, T. *et al.* in *Proc. IODP. 320/321. Integrated Ocean Drilling Program Management International, Inc.*   (ed H. Pälike, Nishi H. Lyle M. Raffi I. Gamage K. Klaus A. and the Expedition 320/321 Scientists,) (2012).

39   Archer, D. Modeling the calcite lysocline. *Journal of Geophysical Research-Oceans* **96**, 17037-17050, doi:10.1029/91JC01812 (1991).

40   Calcagno, P. & Cazenave, A. Subsidence of the sea-floor in the Atlantic and Pacific Oceans - regional and large-scale variations. *Earth and Planetary Science Letters* **126**, 473--492, doi:10.1016/0012-821X(94)90125-2 (1994).

41   Pagani, M. *et al.* The Role of Carbon Dioxide During the Onset of Antarctic Glaciation. *Science* **334**, 1261-1264, doi:10.1126/science.1203909 (2011).

PEAT carbonate accumulation rates and CCD

Legend:
- U1331
- U1332
- U1333
- U1334
- U1335
- U1336
- U1337
- U1338
- ODP1218
- ODP1219
- ODP1220
- ODP1215
- ODP1217
- DSDP574
- DSDP70
- DSDP69
- CCD

MAR   CAR
(mg cm^{-2} kyr^{-1})
- 500
- 1500
- 2500

palaeodepth (km)

benthic $\delta^{18}O$ (‰)

benthic $\delta^{13}C$ (‰)

atmospheric pCO_2
- Phytoplankton
- Stomata
- Boron $\delta^{11}B$
- Paleosols
- Nahcolite
- Liverworts

2,224ppm
1,112ppm
556ppm
278ppm

8x
4x
2x
1x

Labels on plot: MECO, EECO, PETM, CAE-1, CAE-2, CAE-3, CAE-4, CAE-5, CAE-6, CAE-7, E/O

Magnetochrons: C1n, C3n, C5n, C6n, C6Cn, C9n, C13n, C18n, C20n, C21n, C23n

age (Ma)
0   5   10   15   20   25   30   35   40   45   50   55

equatorial Pacific CCD (m)